17èmes JOURNEES DE L'HYDRODYNAMIQUE
JH2020

24 - 26 novembre 2020
CHERBOURG - en - COTENTIN

EXPERIMENTAL AND NUMERICAL STUDY OF A VERTICAL AXIS TURBINE FOR WEC APPLICATION

17emes JOURNEES DE L'HYDRODYNAMIQUE JH2020

V. Podeur[(1),(2),*], Y-M. Scolan[(2)], and T. Santagostini[(1)]

[(1)]Geps Techno, Guérande, France
[(2)]Institut de Recherche Dupuy de Lôme, ENSTA Bretagne, Brest, France
[*]Corresponding author: vincent.podeur@geps-techno.com

Résumé

L'industrie maritime essaye, à tous les niveaux, de réduire de façon croissante son empreinte carbone. L'un de ses défis est de réduire ses besoins en groupes électrogènes pour les applications offshore. Une alternative consiste à produire l'énergie requise sur place via des systèmes houlomoteurs. Cependant, le dimensionnement de tels systèmes requière l'utilisation de modèles prédictifs qui ne sont pas nécessairement disponibles.

Cette étude vise à développer un tel modèle pour les système basés sur la technologie des centrales hydrauliques à tourbillon. Pour cela, un dispositif expérimental a été développé et est présenté ici. Par le biais de mesures PIV, ce système est étudié avec et sans turbine. Les résultats obtenus montrent que l'écoulement est majoritairement irrotationnel et qu'une relation linéaire existe entre l'intensité du tourbillon en amont de la turbine et la hauteur d'eau présente dans le système à débit constant. Un code numérique, basé sur un modèle simple de type distribution de singularités 2D, a été développé. Ses résultats sont comparés aux mesures expérimentales. La puissance calculée par le code surestime par un facteur 2 la puissance réellement développée lors des essais. Cependant, la prise en compte des variations 3D du profil de vitesse radiale doit améliorer ces résultats.

Summary

The maritime industry is increasingly trying to reduce its CO_2 foot-print at every level. One of its challenge is to reduce its need for diesel engine generators in offshore applications. One alternative is to produce the required energy on site thanks to wave energy converters (WEC). However, correct sizing of WEC for a particular application requires the use of predictive models which are not always readily available.

The present study aims at developing such model for WEC based on gravitational vortex hydropower (GVHP). To do so, an experimental setup was developed and is presented herein. Via PIV measurement, the system is studied with and without the turbine. Results show that the flow is mainly irrotational and linear relationship exist between upstream vortex intensity and water height in the system at constant flow rate. A numerical code based on a simple 2D vortex element method was developed and is compared to experimental results. Computed power is overestimated by a factor 2 but further improvement can be expected by taking into account 3D effects in the radial velocity profile.

1. Introduction

Thanks to increasing awareness in the maritime industry regarding environmental issues, needs for cleaner and efficient energy sources are growing. Companies are trying to reduce their CO_2 foot-print, which for most of them in the maritime sector, come from the use of fuel deriving from oil. One of the challenge in reducing the fuel consumption is to get rid of engine-generators used on remote islands or on offshore facilities. An answer to this particular problem is to make use of renewable energies available on-site. At sea, the primary sources are the sun and waves. Whereas solar energy harvesting is a rather simple task thanks to the readily available solar panel technologies, wave energy harvesting through wave energy converter (WEC) is on another level of complexity. The literature shows that a wide variety of WEC concept exist [1], each having advantages and drawbacks, different power output and operational constrains. Therefore, finding the best match between solar and WEC technologies, that can fit in the same structure in a simple and sturdy manner, is not an easy task. Within this context, Geps Techno company develops autonomous platforms used in various offshore contexts such has measurements of wind and current or on-site energy production for oil and gas applications. One of the key features of this platform is its embedded WEC which uses the same principle as gravitational vortex hydropower (GVHP) [2]. It uses a vertical axis turbine (VAT) to harvest the energy from a gravitational vortex generated inside a tank and induced by incoming waves. Such platform requires careful sizing of the WEC during the design process to ensure that the power output meets the application requirement. To do so, in-house tools have been developed at Geps Techno but they only provide crude estimate of the expected power output. Unfortunately, literature on GVHP is scarce and mainly focuses on parametric analysis [3–6]. Moreover, due to the singular nature of the bathtub vortex flow, existing VAT modeling strategies are not well suited for the present device. Thus a relevant model for the considered WEC should be build to improve the reliability of power prediction. The first step toward this goal is to primarily focus on the stationary operation of the system. For this, an experimental apparatus has been built to provide better understanding of the phenomenon at play and data to perform validation of the models. In parallel, a numerical model of the turbine has been developed.

A description of the experimental apparatus and the measurement techniques used will be given in section 2. Then, the numerical model is briefly presented in 3. Finally, salient results from the experiments and a comparison between numerical and experimental results is given in section 4.

2. Experimental apparatus

2.1 General description

The setup for this project is based on the one used in [7]. As explained in the introduction, the goal of this system is to create a steady bathtub vortex inside a partially cylindrical tank where a VAT turbine is installed. A schematic description of the experimental setup is given in figure 1. The key feature of this system is its vortex box, built out of acrylic glass. Such material has the advantage of being transparent and colorless, which is ideal for non-invasive flow visualization techniques such as particle image velocimetry (PIV). General dimensions of the vortex box are given in figure 2. Its shape is 3/4 cylindrical with the remaining 1/4 being occupied by the inlet and a horn which makes the flow converge through a narrower gap when entering the vortex box. The shape of the horn is a portion of a cylinder with a radius equal to the outer one of the vortex box. The outlet diameter of the tank can be easily changed thanks to a circular cutout of 268 millimeter in diameter, in the bottom of the tank. Regarding the cylindrical nature of the tank, one can argue that such shape is not optimal for studying bathtub vortex flow. As explained in [8], tank shape should ideally be of logarithmic nature to ensure a centered and axially symmetrical vortex. Nevertheless, a cylindrical shape is easier to manufacture and is closer to what can be seen in Geps Techno WEC but also in the literature regarding GVHP [5, 6]. The question of flow asymmetry induced by the shape of the tank and the presence of the horn will be addressed later in this paper. The inlet of this box is attached to a U shaped feeding channel of rectangular cross section. A set of four grids are placed in it, right before the vortex box inlet, to act as flow straighteners and homogenizers.

Both parts are installed on an elevated structure to give space between the vortex box and the main tank for the image acquisition setup. To avoid water spillage between upper and lower part of the system, a simple tube is connected to the box outlet. This tube then enters in a rudimentary bubble trap to prevent excessive water aeration. Water is pumped from the tank to the feeding channel thanks to two centrifugal pumps. Two Venturi type flow meters are installed on both feeding line. A Power Take Off (PTO) is installed on top of the vortex box and is used to impose the rotational speed of the turbine. The PTO consists in a brushless motor coupled to a gear box. Rotation speed of the motor is controlled by an Odrive electronic card. The turbine is then linked to the gear box thanks to a shaft guided through a guiding block by two low friction bearing. The top bearing used in this setup is a deep throat ball bearing which can withstand the axial forces exerted by the weight from the turbine and the PTO, without excessive friction loss. Rotation of the PTO is stopped thanks to a lever arm fixed on the gear box frame and a mechanical stop installed on the guiding block. Such setup is used to provide an inexpensive but reliable way to measure dynamical torque acting on the turbine shaft thanks to a simple force sensor installed between the lever arm and the mechanical stop.

The turbine used for this study has an outer radius r_1 of 152 mm where the leading edges of the blades are sitting. Their trailing edges are siting on the inner radius r_2 at a value of 95 mm. The angle of incidence of each blade is -15°. This angle is taken with respect to the radius r_1 of the geometry with the center of rotation being at the intersection of the radius r_1 and corresponding circle perimeter. The tank is linked to a Cartesian reference frame $R_0 = (0, \vec{x}, \vec{y}, \vec{z})$ which origin 0 is located at the center of the outlet. Vectors $\vec{x}$ and $\vec{y}$ are both sharing the same plane at the bottom of the tank. Their orientation is given in figure 2. Vector $\vec{z}$ is pointing upward. The turbine rotation is clockwise with respect to the $\vec{z}$ and is seating at about 12 mm from the bottom of the tank. Blade profile is a NACA 0012 with a chord length of 62 mm and a span of 250 mm.

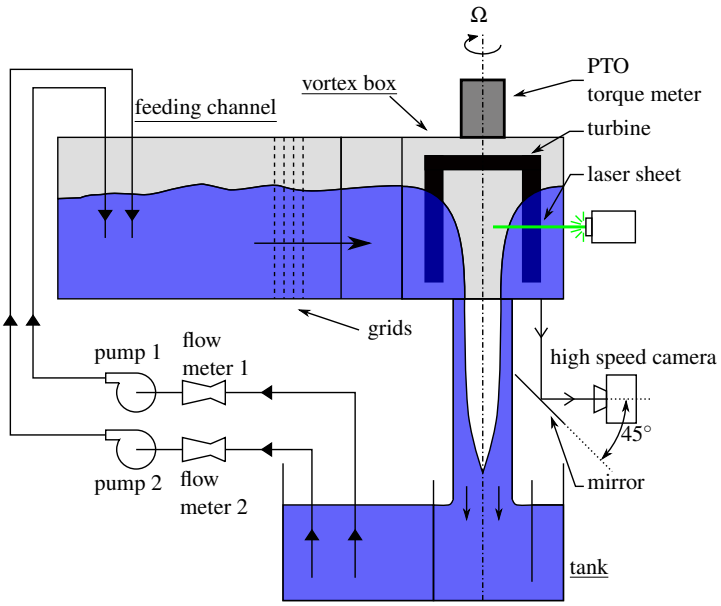

Figure 1. Schematic descritpion of the experimental system.

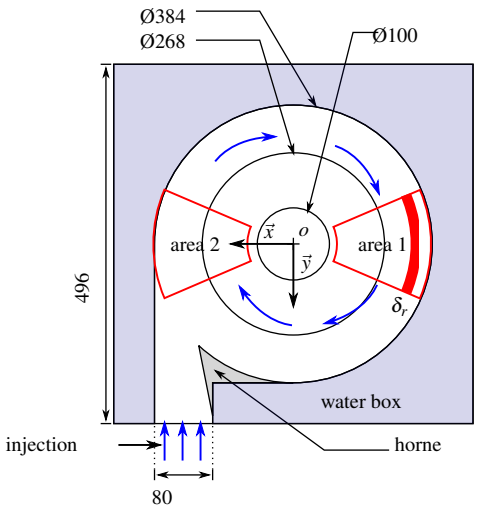

Figure 2. General dimension of the vortex box and location of both area of interest for PIV measurements.

2.2 PIV setup

PIV is used for this experiment. Compared to other single-point flow measurement apparatus, such as Laser Doppler Velocimetry (LDV) of Pitot probes , PIV provides non-intrusive measurements of flow velocity over a wider area.

The image acquisition system for this experiment consists in a pole fixed to a wheeled mount for easy transport. Two extensible arms are fixed to this pole thanks to adjustable pivots. A general schematic of the

system is given in figure 3. The lower arm is supporting the high-speed camera in association with a 45° angled mirror, is positioned below the vortex tank. The upper arm is supporting two laser-sheets modules and is positioned next to the vortex tank. Each module is composed of a 200mW laser of 532nm wave-length, a focalisation lens and a Powell lens which is used to generate the laser sheet. Contrary to cylindrical ones, Powell lens has the advantage of evenly spreading the power across the beam. The fan angle used for our application is of 45° for both modules. The need for having two laser sheets comes from the will to reduce the effect of the shade induced by blades motion. Both leading direction of laser sheets are converging, which induces an overlap of the illumination area. Thus, whatever the angular position of the turbine is, laser sheet obstruction is kept to a minimum and meaning-full information regarding the flow between two blades and downstream the turbine can be gathered. Both arms of the pole are positioned to be parallel to the plan of the tank's bottom. The adjustable pivot of the lower arm is fine-tuned to ensure that the camera angle through the 45° angled mirror is perpendicular to the bottom. Fine-tunings is also done with the upper arm and laser modules to ensure that both laser sheets are co-planar and parallel to the tank bottom. In the end, the effective area of measurement is of 1/8 of the tank which is equivalent to the gap between two blades. A schematic representation of a typical area of measurement is given in figure 2.

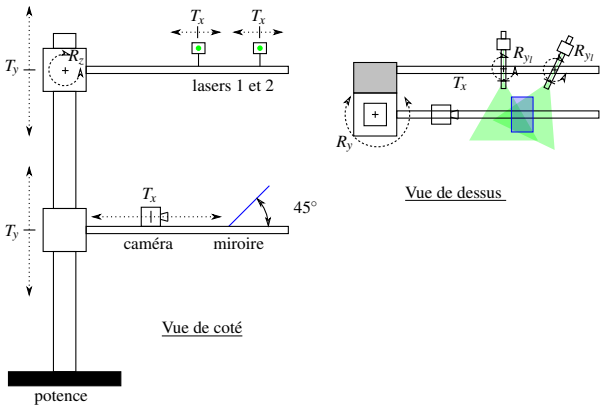

Figure 3. Schematic description of the PIV system

The calibration process consist in using a small checker board positioned at various known heights inside the full vortex tank. The checker board is glued on a cylindrical support which can be precisely set to a known distance inside a PMMA tube. This tube is then put perpendicular to the bottom of the tank so the checker board sit at the desired height while being parallel to the bottom. Several pictures of the calibration target are then taken, at various position in the area of interest for several heights. A typical calibration process implies 5 to 10 pictures for a given altitude in the tank, with this altitude ranging from 5 cm to 30 cm with a step of 5 cm. In the end, the pixel to centimeter ratio is computed for every height, thanks to a camera calibration tool available in Matlab. A typical calibration curve, giving the evolution of the pixel to centimeter ratio with respect to height z, is given in figure 5. On this curve, the effect of perspective can be observed with a decrease of the pixel to millimeter ratio as the height z increases. A significant decrease of 25% in resolution is observed between the minimum height of 5 cm and the maximum one of 30 cm, which nevertheless does not impact the quality of the results during the PIV analysis. Special attention is given to the possible influence of the optical distortion induced by the camera lens. The primary indicator of deformation is the induced skewness of the checker board. It can be evaluated by making use of the camera calibration results. For each calibration picture, corner points of the target are detected. They are identified on figure 4 by a dot. For every square, 3 corner points can be selected to create 2 adjacent vectors $\vec{s_1}$ and $\vec{s_2}$ which share the same origin on one corner of a square. These vectors $\vec{s_1}$ and $\vec{s_2}$ are represented in black and gray respectively on figure 4. These vectors are set to unity and the cross product of $\vec{s_1}$ and $\vec{s_2}$ for every square is computed. The value of this cross product gives the amount of skewness of each square, with the reference value being 1. Investigations show that the median value for the cross product is 0.99999, which means that one half of the squares have one corner between 90° and 89.7°. The mean value is 89.37° and the minimum value is typically of the order of 87.4°. Since the corner detection has an uncertainty of 1 pixel in x and y direction, the induced angle uncertainty δ_α can be computed as the adjacent angle of the longest side $L_{checker}$ of a right-angled triangle with its smallest side being of 1 pixel, where $L_{checker}$ is the length in pixels of a square side for a given height. δ_α is given in equation (1).

$$\delta_\alpha = atan\left(\frac{1}{L_{checker}}\right) \tag{1}$$

This equation gives a value of 2.4° for z equal 30 cm and 1.8° for z equal 5 cm. They are on par with what is

observed regarding the variation of squareness of the checker-board elements.Thus, it can be concluded that the camera lens introduces no perceptible deformation. Variations regarding the squareness of checker-board elements solely arise from the image resolution and the uncertainty in corner detection.

Regarding flow visualization, a Chameleon 3 high-speed camera from Point Grey is used. The specific setup of the camera for this experiment is a resolution of 800×600 pixels and a frame rate of 500 fps. Exposure time is fine-tuned to ensure decent illumination while keeping blur effects to a minimum. Laser illumination is kept constant.The seeding particles used are from Lavision and are made of Polyamide. Their density is of 1.02 g/cm^3 and their diameter is of 60 μm, which ensure a very low sedimentation speed with a good light scattering.

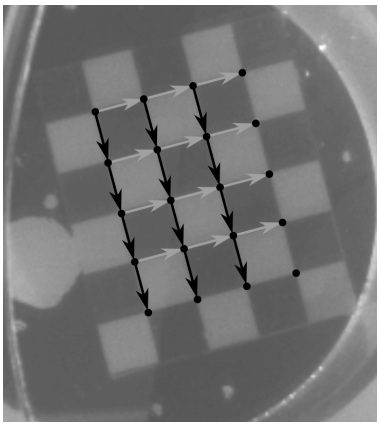

Figure 4. Picture of the calibration target after corner detection process.

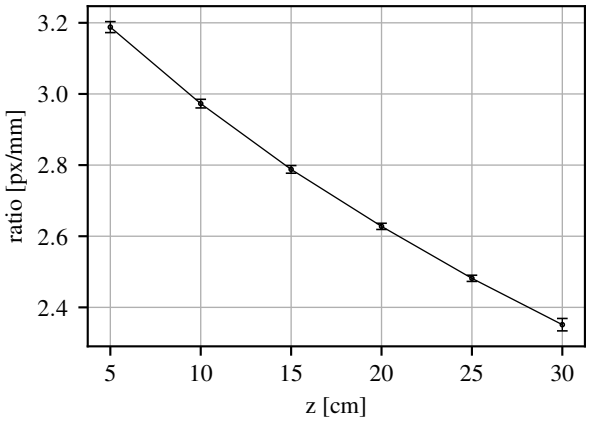

Figure 5. Calibration curve which gives the pixel to millimeter ratio as a function of height z.

2.3 PIV analysis and results post-processing

As mentioned earlier, PIVLab program is used. To analyze the flow, the Discrete Fourier Transform technique is selected. A set of pictures is treated as a sequence, which means that a cross correlation is performed on pictures n and $n+1$, then on pictures $n+1$ and $n+2$ and so on. Thus, for a time series of N pictures, N-1 flow field can be computed. Three passes over one image pair are performed. The first one is performed with a window of 64×64 pixel and the second and third ones with a window of 32×32 pixels. The first larger window is used to increase the spatial resolution in order to accommodate for the larger particle displacement, as suggested in [9]. The other two passes are performed to increase the noise to signal ratio and thus facilitate the detection of the correlation pic. This technique is recommended in [10]. For further information on PIVLab, the reader may refer to [11].

The data obtained from these PIV analysis are then post-processed in two distinct ways. The first one is a simple vector field visualization by subtracting the turbine rotation to provide information regarding the flow in the relative frame off reference attached to the turbine. The second post processing strategy is based on flow field averaging. This approach is only possible because of the steadiness of the present flow. The flow speed is averaged with respect to time and space over a portion of the area of interest. This area is $1/8^{th}$ of an annulus with a thickness δ_r. An illustration of this portion of annulus, of thickness δ_r, is represented on figure 2 by a thick line in area 1.

3. Potential flow model

As observed in [7, 8, 12], bathtub vortex flow is mainly two-dimensional outside its viscous core, with a radial component pointing towards the axis of rotation of the vortex, and a tangential component as well. Moreover, the nature of the flow in this region is globaly irrotational. By neglecting the influence of viscosity, potential

flow theory can be used to build a model. The reasons for using a potential flow model is of computational savings order. The present numerical model is inspired by [13, 14], thus only an outline of the model is given in the next section. More details regarding the turbine rotation and the notion of relative eddy are given in section 3.2.

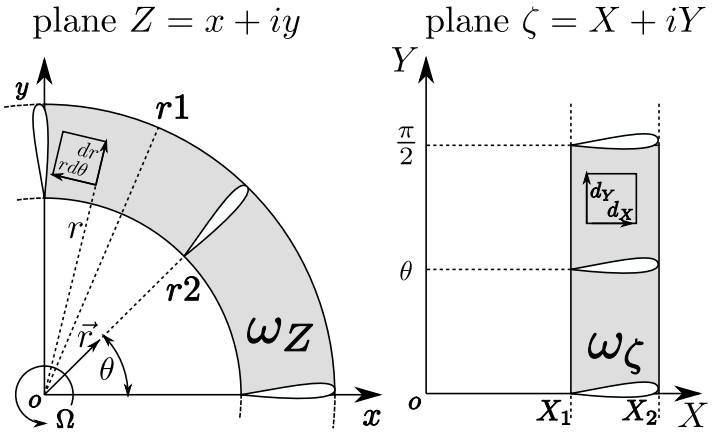

Figure 6. Transformation of the turbine into a straight cascade in ζ plane.

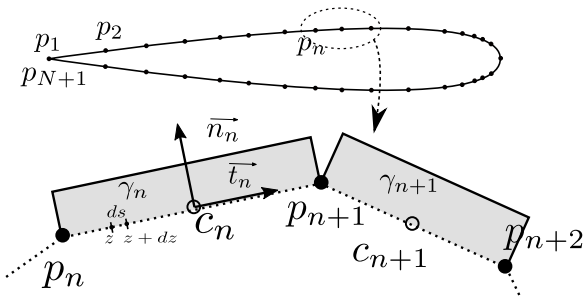

Figure 7. Discretization of the blade into finite set of panels.

3.1 Turbine modeling through conformal mapping

The turbine is modeled thanks to a singularity distributions method and is considered 2D. The shape of the blade is modeled with a finite set of N panels delimited by $N+1$ points as described in figure 7. Its center of rotation seats at the origin of the complex plane Z as described in figure 6. For the sake of practicality, complex notation is adopted. This turbine is immersed inside a bathtub vortex flow which can be modeled thanks to the superposition of a sink flow and a point vortex. A way to simplify the problem is to unwrap it by using the classical transformation $\zeta = ln\, z$. This transformation has tow advantages. Firstly, it turns the free flow complex velocity into a rectilinear and uniform flow C_{∞_ζ}

$$C_{\infty_\zeta} = \frac{m}{2\pi} - i\frac{\Gamma}{2\pi} \tag{2}$$

where m and Γ are the intensity of the sink and the vortex respectively. Secondly, the turbine can be transformed into a straight cascade, as presented in [13, 15, 16]. in a plane ζ. It is a well-known problem where the problematic of blade periodicity as already been tackled [13, 17]. Moreover, the introduction of periodicity further simplify the numerical problem by only requiring the discretization of a single blade profile. After performing the plane change, a constant strength vortex elements of unknown intensity γ_n is distributed on every blade panel. This intensity is determined by imposing the boundary condition on the blade profile. Boundary conditions on the surface blade are defined by two components which are the free flow C_{∞_ζ} and the turbine rotation C_Ω. Since a no-flow condition is desired across the panels, the following relation for one panel can be written as follows

$$Im\left\{\left(C_{\infty_\zeta}(c_n) + C_\Omega(c_n) + \sum_{m=1}^{N}\gamma_m a_{n,m}\right)\frac{z_{p_{n+1}} - z_{p_n}}{|z_{p_{n+1}} - z_{p_n}|}\right\} = 0 \tag{3}$$

with $a_{n,m}$ the influence coefficient of element m over element n, γ_m vortex intensity of element m and $z_{p_{n+1}}$, z_{p_n} the complex coordinates of the end points of panel n. Equation (3) is given in the panel reference frame at its center c_n thanks to the rotation $\frac{z_{p_{n+1}} - z_{p_n}}{|z_{p_{n+1}} - z_{p_n}|}$. In the end, a linear system of equations of the form $A\gamma = B$, with A being the influence coefficients matrix of size $(N \times N)$, B the boundary conditions for the N panels of size $(N \times 1)$ and the unknowns matrix γ of size $(N \times 1)$. Prior to solving the system, the Kutta condition should be

imposed by forcing the intensity on both upper and lower panels of the trailing edge to be equal in norm but opposite in sign, yielding

$$\gamma_1 + \gamma_N = 0 \tag{4}$$

As presented in [13, 14], many strategies can be selected to impose this condition. In the present method, the kutta condition is simply added to every line of A. Finally, the complex speed C_{f_ζ} of the flow at a given point ζ in plane ζ is given by equation (5).

$$C_{f_\zeta}(\zeta) = C_{\infty_\zeta} + C_{\Omega_\zeta}(\zeta) + \sum_{n=1}^{N} C_{b_\zeta}(\gamma_m, \zeta) \tag{5}$$

with $C_{b_\zeta}(\gamma_m, \zeta)$ being the speed induced by vorticity panel m.

3.2 Turbine rotation and relative eddy

Unlike axial flow turbine, the effect of rotation for a radial flow one cannot be modeled with a simple translation in ζ plane. Since the turbine motion can be compared to a solid-body rotation, it cant be introduced in ζ plane through a conformal mapping. Doing so would mean having the leading edge translating at a higher speed than the trailing edge in the Y direction.

The solution proposed in [16] is to consider the flow relative to the turbine. In the rotating frame, attached to the turbine, a relative vorticity ω_Z of magnitude 2Ω appears, as a result of the turbine angular velocity Ω. This vorticity is linked to the relative eddy which is present between blades when flow is observed in the rotating frame. This vorticity ω_Z can be transformed into a relative vorticity ω_ζ in plane ζ by applying the circulation theorem over two equivalent differential elements visible in figure 6, which gives

$$\omega_Z r\, dr d\theta = \omega_\zeta dX dY \tag{6}$$

where

$$\frac{dr}{r} = dX \qquad\qquad d\theta = dY \tag{7}$$

so that

$$\omega_\zeta = 2\Omega e^{2X} \tag{8}$$

Then, vorticity ω_ζ can be linked to the curl of the flow in plane ζ, which leads to equation (9).

$$\frac{\partial V}{\partial X} = 2\Omega e^{2X} \tag{9}$$

after integration of (9) with respect to X, we get equation

$$V_\Omega = \Omega e^{2X} + C \tag{10}$$

where C is a constant of integration.

Since the vorticity is continuously distributed over the cascade, between the leading edge position X_1 and the trailing edge X_2, it can be seen as a vortex line of finite thickness $\delta_X = X_1 - X_2$, stretching from $-\infty$ to ∞. Due to symmetry, $V_\Omega(X_1)$ and $V_\Omega(X_2)$ are equal in norm but opposite in sign. Hence yielding

$$\Omega e^{2X_1} + C = -\Omega e^{2X_2} - C \tag{11}$$

which gives the value of constant C

$$C = -\frac{\Omega}{2}\left(e^{2X_1} + e^{2X_2}\right) \tag{12}$$

Finally, complex perturbation speed c_{Ω_ζ}, induced by the relative vorticity ω_ζ, is given in

$$c_{\Omega_\zeta} = -i\left(\Omega e^{2X} - \frac{\Omega}{2}\left(e^{2X_1} + e^{2X_2}\right)\right) \tag{13}$$

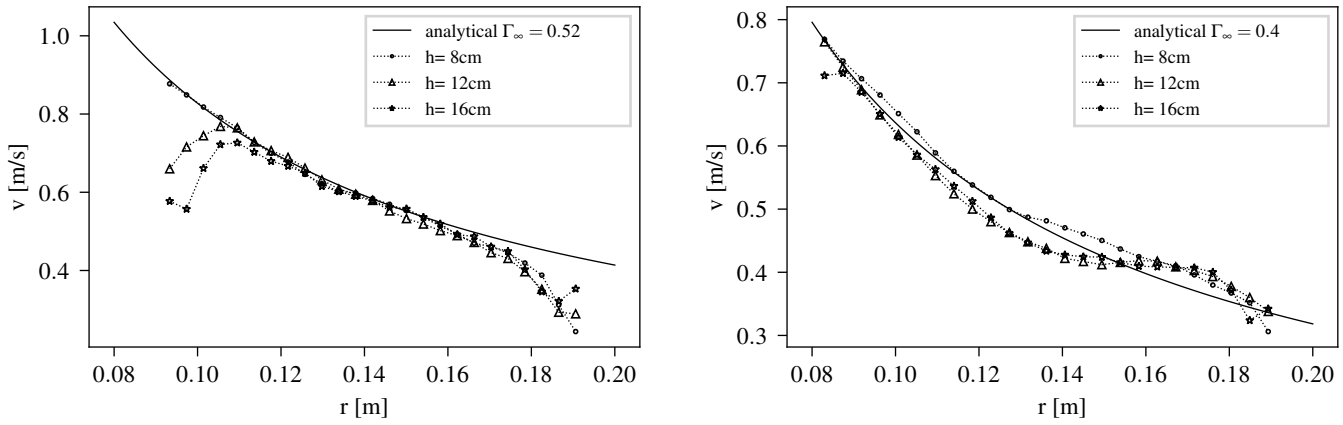

(a) **(b)**

Figure 8. Results from experiments without turbine. The legend gives the height h of the laser sheet with respect to the bottom of the tank in centimeters. **(a)** Tangential speed profile, area 1. **(b)** Tangential speed profile, area 2.

4. Results

In this section, results from PIV measurements are shown and analyzed. Firstly, results without the turbine are presented in order to characterize the free vortex flow and evaluate its symmetry. Secondly, results with the turbine are analyzed. Finally, a comparison between numerical and experimental results is performed.

4.1 Bathtub vortex without turbine

PIV measurements without the turbine are performed at constant flow rate Q of $4.15\,l/s$ for area 1 and 2. The goal of these measurements is to characterize the nature of the flow in the system prior to introducing the turbine. For a given area, PIV measurements are performed for several heights over a period of one second with a frame rate of 500 fps, which means that 499 image pairs where available for analysis.

The averaged tangential speed profile for area 1 and 2 are given in figure 8a and 8b. These profiles are obtained at three different heights from the bottom of the tank with its center seating at $r = 0$, where the center of the vortex is approximately localized. In both figures, an analytical model of the classic potential point vortex $\Gamma/2\pi r$ is fitted.

For area 1, it appears that the velocity profiles are independent of the height z. Regarding the velocity variation with respect to r for $h = 12\,cm$ and $16\,cm$, it increases until reaching a maximum of $0.74\,m^2/s$, around $r \approx 0.1\,m$, and then steadily decreases up to $r \approx 0.17\,m$ where a sudden decrease happens. For $h = 8\,cm$, the velocity steadily decreases right from the first value until $r \approx 0.17\,m$ where a sharp decrease also happens. The differences regarding the beginning of the curves can be explained by the presence of the vortex air core and its surrounding viscous layer, as represented in the Rankine's vortex model. Due to the funnel shape of the air core, the viscous part of the vortex is shifted toward larger r value as altitude increases. Regarding the sharp velocity decrease at $r \approx 0.17\,m$, its origin is due to the presence of a boundary layer at the vertical wall of the tank. In between the viscous and the boundary layer, all three profiles show a very good agreement with the analytical solution of the potential point vortex, which highlights the fact that the bulk of the flow is truly irrotational.

For area 2, the velocity decreases monotonically with respect to r for all three data sets. The rate of decrease slows down around $r = 0.14\,m$ where a plateau is reached for $h = 12, 16\,cm$. This feature is not present for $h = 8\,cm$. After $r \approx 0.17\,m$, a sharp decrease for all three curves is observed. This characteristic can be attributed to the presence of a boundary layer on the tank wall. Regarding the dependency with height z, it appears that velocity profiles for $h = 12\,cm$ and $16\,cm$ are identical but variations can be observed for $h = 8\,cm$. These variations are mainly visible around $r = 0.14\,m$. Hence, the dependency with z is deemed to be not significant. Unlike area 1, the present results do not agree well with the analytical solution. The

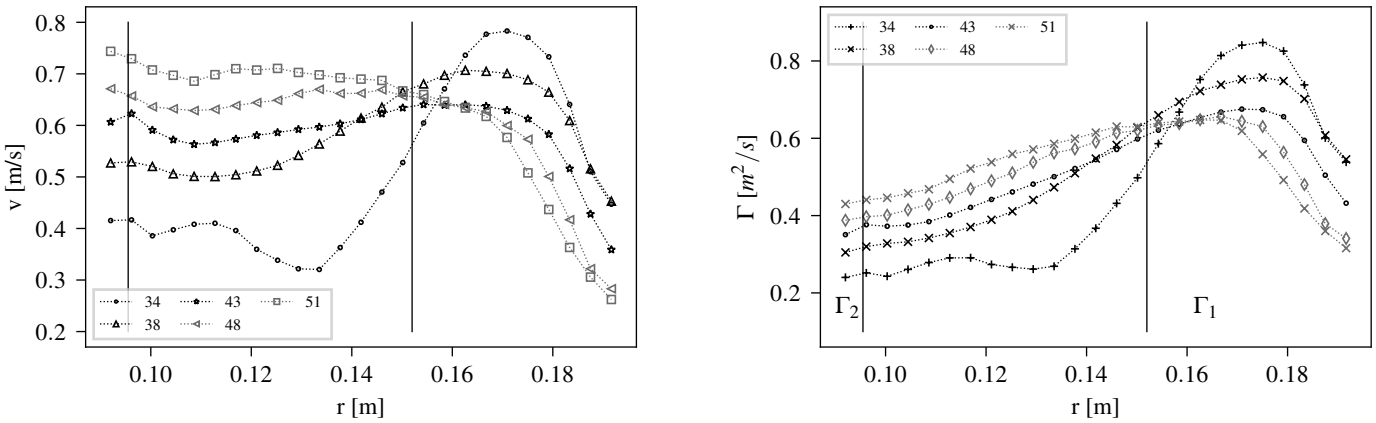

(a) **(b)**

Figure 9. Results from experiments with turbine. The legend gives the rotational speed of the turbine in rotations per minutes (rpm). Measurements height for the laser sheet is 8 centimeters. **(a)** Tangential speed profile, area 1. **(b)** Circulation profile, area 1.

best agreement between analytical and experimental results occurs for $r < 0.11\,m$. The discrepancy between experimental and analytical results for area 2 are mainly due to the presence of the inlet in the vicinity of measurement area.

From these observations, it emerges that the flow inside the tank without the turbine is mainly irrotational in area 1 and partially irrotational in area 2. This confirms the relevance of choosing a numerical code based on potential flow theory. Even though the tank is almost cylindrical, its inlet has a significant influence on the shape of the free vortex which induces an asymmetry inside the flow. These observations are of importance for the future numerical / experimental comparison. Regarding radial flow, despite significant effort during the post-processing stage, no relevant information was obtained. Whatever the measurement, no obvious trend can be identified. The same difficulty was encountered in [8].

4.2 Vortex with turbine at constant flow rate

Measurements with the turbine are performed for various rpm with a constant flow rate Q of $4.15\,l/s$, with an illumination plane set at $8\,cm$ from the bottom of the tank. The length and frame rate of PIV measurements is the same as for section 4.1.

The averaged tangential speed profile for area 1 is given in figure 9a. Outer and inner radius r_1 and r_2 of the turbine are represented on this figure by two vertical lines. Velocity profiles are given for five values of rpm, ranging from 34 to 51 rpm. Regarding general evolution of the velocity profile, two significant behaviors can be observed. First, for interval $[r_1, r_t]$, with r_t being the radius of the tank, velocities increase with the rotational speed. The highest speed is observed for 51 rpm and the lowest for 34 rpm with every other rotational speeds in-between in ascending order. This trend is inverted for interval $[r_2, r_1]$ where the highest velocity profile is obtained for 51 rpm and the lowest for 34 rpm.

An easier way to analyze these results is to consider the local circulation Γ, by multiplying the velocity profiles by $2\pi r$. This local circulation gives the evolution of the vortex intensity Γ with respect to the radius r. Doing so for the free vortex results presented in section 4.1, gives a straight line over the potential part of the results. The local circulation with respect to r is given in figure 9b. For all rpm except rpm 34, the circulation increases with respect to r until it reaches a small plateau after r_1. After this plateau, the circulation sharply decreases due to the presence of the boundary layer at r_w. The difference between Γ_1 upstream and Γ_2 downstream is decreasing while the turbine speed increases. This observation should be linked to the evolution of torque with respect to rotational speed given in figure 10a. It appears that the torque decreases with respect to the rotational speed ω which means that torque is proportional to upstream-downstream circulations differences. These observations are in agreement with the Euler pump equation $T = \frac{\rho Q}{2\pi}(\Gamma_1 - \Gamma_2)$, where the

torque generated by the fluid on the turbine depends solely on the difference $\Gamma_1 - \Gamma_2$ for constant Q. The later observations can also be made for measurements obtained in area 2.

Upstream and downstream circulations Γ_1 and Γ_2 are plotted in terms of water height h_t in the tank in figures 11 and 12 for area 1 and area 2 respectively. For both area, Γ_1 decreases linearly with respect to h_t while Γ_2 increases linearly. For area 1, the mean value $(\Gamma_1 + \Gamma_2)/2$ is computed and remains constant for every values of h_t and is equal to the vortex intensity Γ_∞ obtained for area 1 with no turbine, given in figure 8a. Another feature of this figure is that both linear fits of Γ_1 and Γ_2 intersect for $\Gamma = \Gamma_\infty$ and $h_t \approx 1.05\, h_{t\infty}$. The same features appear in figure 12 except that $(\Gamma_1 + \Gamma_2)/2$ is not constant anymore. Linear fits of Γ_1 and Γ_2 intersect for $\Gamma = 0.9\,\Gamma_\infty$ and $h_t \approx 1.03\, h_{t\infty}$. These results highlight that upstream circulation Γ_1 follows a linear law with respect to the water height h_t, which is valuable for extrapolating data when PIV measurements are prohibited due to insufficient water level in the tank. Regarding the discrepancies between figures 11 and 12, they can be explained by the influence of the inlet in area 2. The fact that the same features can be observed in both graphs shows that the bulk of the flow experiment some skewness due to the inlet while keeping its key features. As suggested by Mulligan [8], a tank with a logarithmic shape would have been an efficient way to keep the flow symmetrical. Unfortunately such a tank was not available for this experiment. The same comment as for section 4.1 can be made about radial velocity profiles not being exploitable.

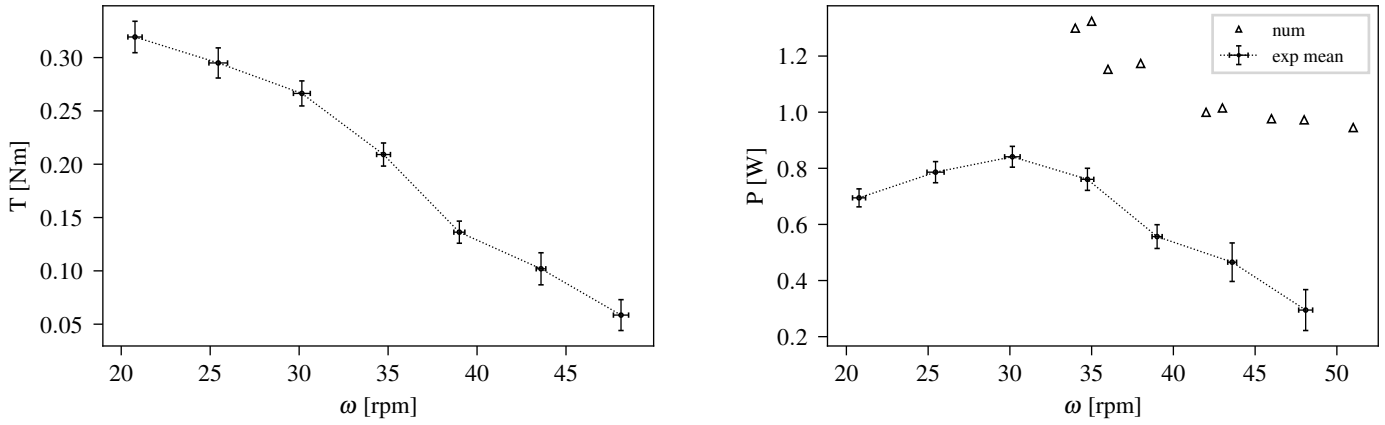

(a) **(b)**

Figure 10. Each point of the experimental curves are obtained by averaging the measured torque and rotational speed over 10 runs of 1 minute length at a rate of $10Hz$. Horizontal and vertical stem are the associated standard deviations. **(a)** Evolution of measured mean torque T with respect to rotational speed ω. **(b)** Evolution of measured mean Power T, with respect to rotational speed ω, compared to numerical results.

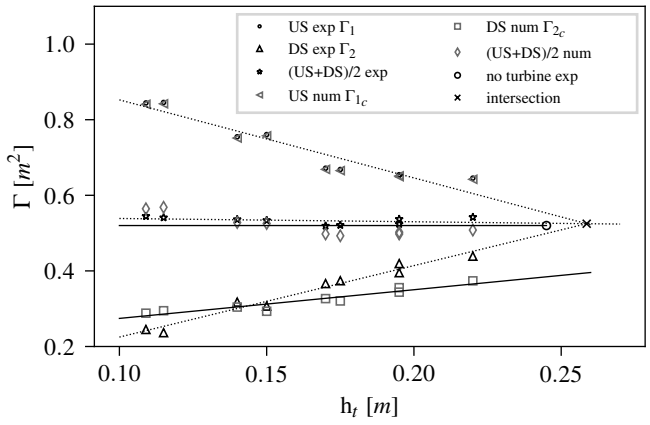

Figure 11. Γ_1 and Γ_2 variation with respecto h_t for area 1. US=upstream, DS=downstream

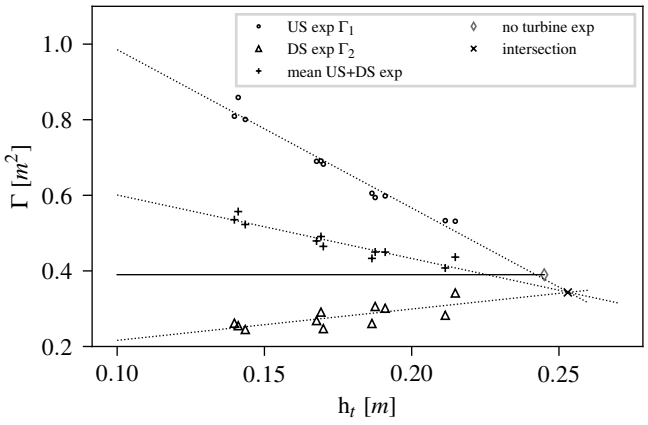

Figure 12. Γ_1 and Γ_2 variation with respecto h_t for area 2. US=upstream, DS=downstream

4.3 Comparison between numerical and experimental results

A purely 2D approach is adopted for this comparison. Experimental results regarding the upstream vortex intensity Γ_1, rotational speed ω and water height h_t for area 1 are taken as inputs for the numerical model. Sink intensity is taken as $m = Q/h_t$. The power generated by the turbine is computed thanks to Euler's equation times the rotational speed ω in rad/sec. The computed power with respect to ω is plotted in figure 10b alongside the experimental results. It is clear that the numerical model, compared to experimental results, overestimates the power output by a factor of approximately 2. Despite significant discrepancies, both results share the same order of magnitude. Evolution of computed down-stream circulation Γ_{2_c} is also plotted in figure 11. It can be seen that Γ_{2_c} increases linearly with respect to h_t but shows a smaller slope compared to the experimental results of Γ_2.

Such discrepancies may be explained by the purely 2D nature of the model. As shown in [12, 18], radial velocity profile is strongly varying with respect to height z, with most of the flow occurring in a thin layer next to the bottom of the tank. these variations of the radial flow will have two effects: Firstly, the angle of attack will vary with z, which may induce changes on the blades loading. Secondly, by taking into account the clearance between the tip of the blades and the tank bottom, the effective flow rate Q_{ef} collected by the turbine will depend on the influence of the bottom flow layer, with Q_{ef} being a fraction of the total flow rate Q. Including these 3D effects are part of an ongoing work and its outcome will be presented in a future communication.

5. Conclusion

Experimental results by means of PIV measurements for a radial flow vertical axis turbine have been presented and compared to a numerical model. A thorough description of the experimental and PIV setup as well as a general description of the numerical model, based on potential flow theory and singularity distributions method are given.

It appears that the tangential velocity in the bulk of the flow, without the turbine, can be modeled with the classical point vortex solution. With the turbine, the local circulation derived from the velocity profile, shows variations in agreement with the well-known Euler pump equation. Further analysis of the local circulation $\Gamma_{1,2}$ upstream and downstream of the turbine, show that both quantity are linearly dependent with respect to the water height h_t in the tank. This dependence is useful for extrapolating upstream circulation and water level h_t when no PIV measurements are available.

Finally a comparison between numerical and experimental results is performed. Numerical results overestimate by a factor 2 the power generated by the turbine. To improve the numerical modeling, proposition about taking into account the radial velocity profile variation with z is made.

Acknowledgments

The authors would like to thanks Julien Le Clanche and Kilian Crocci for their valuable help during the setup of the experiment. The authors would also like to thank Frédéric Montel and Didier Penchenat for their precious technical support and expertise during the early stage of the experiment installation.

References

[1] B. Drew, A. R. Plummer, and M. N. Sahinkaya, "A review of wave energy converter technology," 2009.

[2] A. B. Timilsina, S. Mulligan, and T. R. Bajracharya, "Water vortex hydropower technology: a state-of-the-art review of developmental trends," *Clean Technologies and Environmental Policy*, vol. 20, no. 8, pp. 1737–1760, 2018.

[3] C. Power, A. McNabola, and P. Coughlan, "A parametric experimental investigation of the operating conditions of gravitational vortex hydropower (gvhp)," *Journal of Clean Energy Technologies*, vol. 4, no. 2, pp. 112–119, 2016.

[4] A. S. Saleem, T. A. Cheema, R. Ullah, S. M. Ahmad, J. A. Chattha, B. Akbar, and C. W. Park, "Parametric study of single-stage gravitational water vortex turbine with cylindrical basin," *Energy*, p. 117464, 2020.

[5] C. Christopher, D. Adanta, *et al.*, "The effect of basin geometry on gravitational vortex hydropower," in *IOP Conference Series: Materials Science and Engineering*, vol. 788, p. 012081, IOP Publishing, 2020.

[6] V. J. A. Guzmán, J. A. Glasscock, and F. Whitehouse, "Design and construction of an off-grid gravitational vortex hydropower plant: A case study in rural peru," *Sustainable Energy Technologies and Assessments*, vol. 35, pp. 131–138, 2019.

[7] G. Fourestier, *Modélisation expérimentale et numérique de l'écoulement au sein d'un système convertisseur de l'énergie de la houle*. PhD thesis, Brest, 2017.

[8] S. Mulligan, "Experimental and numerical analysis of three-dimensional free-surface turbulent vortex flows with strong circulation," *Ireland: Institute of Technology Sligo*, 2015.

[9] F. Scarano and M. L. Riethmuller, "Iterative multigrid approach in piv image processing with discrete window offset," *Experiments in Fluids*, vol. 26, no. 6, pp. 513–523, 1999.

[10] J. Westerweel, D. Dabiri, and M. Gharib, "The effect of a discrete window offset on the accuracy of cross-correlation analysis of digital piv recordings," *Experiments in fluids*, vol. 23, no. 1, pp. 20–28, 1997.

[11] W. Thielicke, *The flapping flight of birds: Analysis and application*. PhD thesis, University of Groningen, 2014.

[12] L. L. Daggett, G. H. Keulegan, *et al.*, "Similitude conditions in free-surface vortex formations," 1974.

[13] R. I. Lewis, *Vortex element methods for fluid dynamic analysis of engineering systems*, vol. 1. Cambridge University Press, 2005.

[14] J. Katz and A. Plotkin, *Low-speed aerodynamics*, vol. 13. Cambridge university press, 2001.

[15] R. Bidard and J. Bonnin, *Energétique et turbomachines*. Éditions Eyrolles, 1979.

[16] D. Pollard, "Paper 22: The extension of schlichting's analysis to mixed flow cascades," in *Proceedings of the Institution of Mechanical Engineers, Conference Proceedings*, vol. 180, pp. 86–95, SAGE Publications Sage UK: London, England, 1965.

[17] R. Rey, F. Bakir, and R. Noguera, "Dimensionnement des turbomachines tome i et ii," 1998.

[18] L. Cristofano, M. Nobili, G. Romano, and G. Caruso, "Investigation on bathtub vortex flow field by particle image velocimetry," *Experimental Thermal and Fluid Science*, vol. 74, pp. 130–142, 2016.